An EPR Study of 2,3-Bis(diphenylphosphino)maleic Anhydride (BMA) Complexes and the BMA Radical Anion

Noel W. Duffy,[†] Ross R. Nelson,[‡] Michael G. Richmond,[§] Anne L. Rieger,[‡] Philip H. Rieger,*[,‡] Brian H. Robinson,[†] David R. Tyler,[||] Jian Cheng Wang,[§] and Kaiyuan Yang[§]

Departments of Chemistry, Brown University, Providence, Rhode Island 02912, University of North Texas, Denton, Texas 76203, University of Oregon, Eugene, Oregon 97403, and University of Otago, Dunedin, New Zealand

Received May 22, 1998

EPR spectra are reported for four metal complexes of 2,3-bis(diphenylphosphino)maleic anhydride (BMA), $[Co_2(PhCCR)(CO)_4(\eta\text{-BMA})]^-$, R = Ph, H, $[Co_2(PhCCPh)(CO)_4(\mu\text{-BMA})]^-$, and $[PhCW(CO)_2(BMA)Cl]^-$, as well as the radical anions, $[BMA]^-$ and $[BPCD]^-$, BPCD = 4,5-bis(diphenylphosphino)cyclopentene-1,3-dione. At room temperature, all spectra are 1:2:1 triplets due to hyperfine coupling to two equivalent ^{31}P nuclei with coupling to two equivalent ^1H nuclei for $[BPCD]^-$ and unresolved coupling to one or two ^{59}Co nuclei for the Co complexes with chelating or bridging BMA, respectively. The ^{31}P couplings are temperature dependent, ca. −3 and −13 mG K^{-1} for the metal complexes and ligand radical anions, respectively. At low temperature, the spectrum of $[BMA]^-$ shows the presence of symmetric and asymmetric PPh_2 rotational conformers, related by the thermodynamic parameters $\Delta H° = -0.8 \pm 0.2$ kJ mol^{-1} and $\Delta S° = 4 \pm 1$ J mol^{-1} K^{-1} and interconverted with activation parameters $\Delta H^‡ = 18.2 \pm 0.4$ kJ mol^{-1}, $\Delta S^‡ = -30 \pm 2$ J mol^{-1} K^{-1}. The temperature dependence of the ^{31}P couplings is explained by a negative spin-polarization contribution to $\langle a^P \rangle$ and a positive contribution due to P 3s character; the latter increases with the asymmetry of the PPh_2 conformations. The range of conformations accessible to the metal complexes is less than for the ligand radical anions, and accordingly the temperature dependence is significantly smaller.

Introduction

Several years ago, Mao, et al.,[1,2] reported EPR spectra of $[Co(CO)_2L(BMA)]$, L = CO (**1**), PPh_3 (**2**); BMA = 2,3-bis(diphenylphosphino)maleic anhydride, best described as Co(I) complexes with a BMA radical anion ligand. The spectra exhibited ^{31}P and ^{59}Co hyperfine couplings which are unusually temperature- and solvent-dependent. The ^{31}P coupling increases in magnitude with decreasing temperature while the ^{59}Co coupling decreases in magnitude; both couplings decrease with increasing solvent polarity. Qualitatively similar solvent effects were observed for the C−O stretching frequencies, the lowest energy electronic absorption frequency, and the rate of substitution of CO by PPh_3 in $[Co(CO)_3(BMA)]$. These effects were attributed to stabilization of the $Co^+(BMA)^-$ zwitterion with increasing solvent polarity.

Subsequent work on other metal complexes, reported in this paper, suggests that the above interpretation, while substantially correct with respect to solvent effects, is oversimplified with respect to the temperature-dependent hyperfine couplings. Accordingly, we were led to a study of the free ligand radical anion, $[BMA]^-$, which has greatly added to our understanding of the system.

Here we report temperature-dependent EPR spectra of four BMA complexes, $[Co_2(PhCCR)(CO)_4(\eta\text{-BMA})]^-$, R = Ph (**3a**$^-$), H (**3b**$^-$), $[Co_2(PhCCPh)(CO)_4(\mu\text{-BMA})]^-$ (**4**$^-$), and $[PhCW(CO)_2(BMA)Cl]^-$ (**5**$^-$), in addition to those of the ligand radical anion, $[BMA]^-$ (**6**$^-$), and the radical anion of the related compound 4,5-bis(diphenylphosphino)cyclopentene-1,3-dione (BPCD) (**7**$^-$).

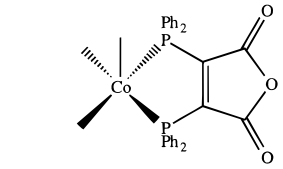

$[Co(CO)_3(BMA)]$ (**1**)

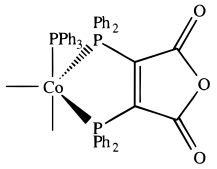

$[Co(CO)_2(PPh_3)(BMA)]$ (**2**)

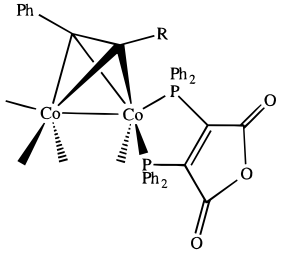

$[Co_2(PhCCR)(CO)_4(\eta\text{-BMA})]$, R = Ph, H (**3a, 3b**)

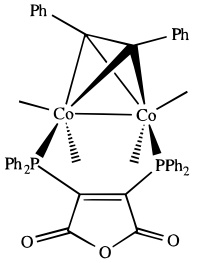

$[Co_2(PhCCR)(CO)_4(\mu\text{-BMA})]$ (**4**)

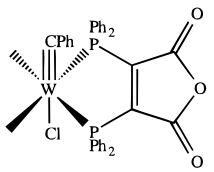

$[PhCW(CO)_2(BMA)Cl]$ (**5**)

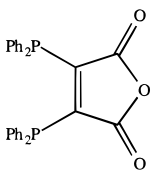

BMA (**6**)

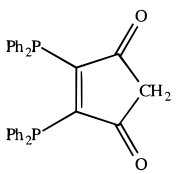

BPCD (**7**)

[†] University of Otago.
[‡] Brown University.
[‡] University of North Texas.
[||] University of Oregon.

(1) Mao, F.; Tyler, D. R.; Rieger, A. L.; Rieger, P. H. *J. Chem. Soc., Faraday Trans.* **1991**, *87*, 3113.
(2) Mao, F.; Tyler, D. R.; Bruce, M. R. M.; Bruce, A. E.; Rieger, A. L.; Rieger, P. H. *J. Am. Chem. Soc.* **1992**, *114*, 6418.

S0020-1669(98)00581-3 CCC: $15.00
Published on Web 09/04/1998

Experimental Section

The ligands BMA (**6**) and BPCD (**7**) were prepared from dichloromaleic anhydride and 4,5-dichlorocyclopentene-1,3-dione, respectively,[3,4] while the $Ph_2P(TMS)$ used in the synthesis of the diphosphine ligands was prepared from PPh_3 and TMSCl.[5] The compounds **3a, 3b**, and **4** were prepared from $[Co_2(CO)_6(alkyne)]$ and BMA according to published procedures.[6,7] The carbyne complex $[PhCW(CO)_4Cl]$ was synthesized according to the procedure of Mayr.[8] All compounds were handled and stored under argon using Schlenk techniques.

$[PhCW(CO)_2(BMA)Cl]$ (5). To a freshly prepared solution of $[PhCW(CO)_4Cl]$ (ca. 1.0 mmol) in THF at −78 °C was added 0.56 g (1.2 mmol) of BMA, after which the solution was allowed to warm to room temperature with stirring continued overnight. IR analysis of the crude reaction solution revealed the presence of the desired BMA-substituted complex. THF was removed under vacuum and the product taken up in 100 mL of toluene, followed by filtration over a short pad of Celite. The solution was concentrated to a volume of ca. 25 mL and then layered with 20 mL of pentane, which ultimately afforded 0.23 g of green-yellow crystals of **5**. Yield: 28%. IR (CH_2Cl_2): ν(CO) 2021 (s), 1958 (s), 1777 (s, BMA). $^{31}P\{^1H\}$ NMR ($CDCl_3$): δ 32.64 (J_{W-P} = 117 Hz). Anal. Calcd (found) for $C_{37}H_{25}ClO_5P_2W$: C, 53.49 (52.54); H, 3.03 (3.46).

Metal BMA complexes, in 1:1 $CH_2Cl_2/C_2H_4Cl_2$, 1:1 $C_2H_4Cl_2$/THF, or THF with 0.1 M $[NBu_4][PF_6]$ or $[NBu_4][ClO_4]$ supporting electrolyte, were reduced electrochemically in situ in the EPR cavity. $\mathbf{6}^-$ was generated by electrochemical reduction in acetonitrile or by $[Co(C_5H_5)_2]$ reduction in THF with qualitatively similar results; because of the greater temperature range accessible with THF, the data presented here are of $\mathbf{6}^-$ in THF. $\mathbf{7}^-$ was generated electrochemically in THF with $[NBu_4][ClO_4]$ supporting electrolyte.

EPR spectra were recorded using a Bruker ER-220D X-band spectrometer equipped with a Bruker variable temperature accessory, a Systron-Donner microwave frequency counter, and a Bruker gaussmeter.

Results and Discussion

BMA Complexes. EPR spectra of $[Co_2(PhCCR)(CO)_4(\eta\text{-BMA})]^-$, R = Ph ($\mathbf{3a}^-$), H ($\mathbf{3b}^-$), and $[Co_2(PhCCPh)(CO)_4(\mu\text{-BMA})]^-$ ($\mathbf{4}^-$), obtained on electrochemical reduction of the neutral parent compounds in THF, 1:2 CH_2Cl_2/THF, or 1:1 $CH_2Cl_2/C_2H_4Cl_2$, are all apparently simple 1:2:1 triplets corresponding to hyperfine coupling to two equivalent ^{31}P nuclei ($I = {}^1/_2$). Typical spectra of $\mathbf{3b}^-$ and $\mathbf{4}^-$ are shown in Figure 1a. Although small extra lines are usually seen in the spectra (see below), the initially formed radical anions appear to be quite stable, consistent with the completely reversible reduction processes observed in cyclic voltammetry.[6]

On close inspection, the lines of the triplet spectra are seen to be grossly distorted from either Gaussian or Lorentzian line shapes. Least-squares analysis of digitized spectra result in very good fits to the line shapes for $\mathbf{3a}^-$ and $\mathbf{3b}^-$ if we assume unresolved hyperfine coupling to one ^{59}Co nucleus ($I = {}^7/_2$); for spectra of $\mathbf{4}^-$, the fit is best assuming hyperfine coupling to two ^{59}Co nuclei. As seen in Figure 1b,c, which compares the central lines of spectra of $\mathbf{3b}^-$ and $\mathbf{4}^-$ with least-squares fits assuming one and two unresolved Co couplings, the distinction

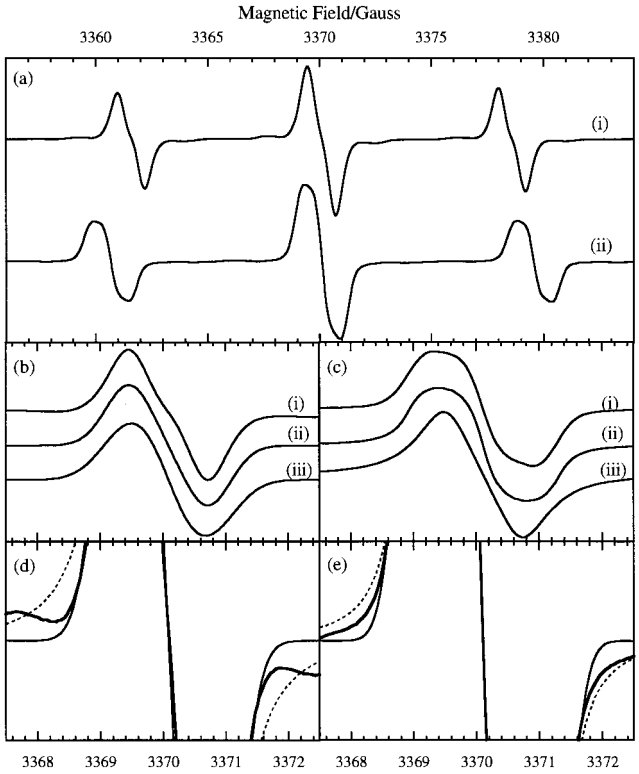

Figure 1. (a) X-band EPR spectra of $\mathbf{3b}^-$ (i) and $\mathbf{4}^-$ (ii) at 210 and 240 K, respectively. (b) Comparison of $\mathbf{3b}^-$ central line (i) with least-squares-fitted simulations assuming one (ii) or two (iii) unresolved ^{59}Co coupling. (c) Comparison of $\mathbf{4}^-$ central line (i) with least-squares-fitted simulations assuming two (ii) or one (iii) unresolved ^{59}Co coupling. (d, e) Comparison of $\mathbf{3b}^-$ and $\mathbf{4}^-$ central lines (heavy lines) with least-squares-fitted simulations assuming Gaussian (solid lines) or Lorentzian (dashed lines) line shapes.

is clear: unresolved coupling to one Co results in sharply defined extrema whereas coupling to two Co nuclei gives more rounded extrema. Since the unpaired electron resides primarily in the maleic anhydride π-system,[1] we expect coupling to only one Co nucleus when BMA is a chelating ligand ($\mathbf{3}^-$) and to two Co nuclei when BMA is bridging ($\mathbf{4}^-$) and can conclude that there is no isomerization of the BMA ligation on reduction.

A total of 28 spectra in the temperature range 200−300 K were subjected to least-squares analysis to determine the solvent and temperature dependence of the ^{31}P and ^{59}Co couplings as well as the component line widths and line shapes for $\mathbf{3a}^-$ (in 1:1 $CH_2Cl_2/C_2H_4Cl_2$, 1:2 CH_2Cl_2/THF, and THF), $\mathbf{3b}^-$ (in THF), and $\mathbf{4}^-$ (in 1:2 CH_2Cl_2/THF). The results are shown in Table 1, which also gives comparable results for **1** and **2** in THF solution.[1]

The distinction between Gaussian and Lorentzian components is subtle and relies on comparison of the wings of the line: Lorentzian component shapes result in broader wings than do Gaussian components. In general, Gausian line shapes are expected if the spectrum is subject to "inhomogeneous broadening", e.g., an unresolved ^1H multiplet or an instantaneous Gaussian distribution of coupling constants; Lorentzian shapes are expected for "exchange-narrowed lines", e.g., when the radical species tumbles sufficiently rapidly to average anisotropies in the g and hyperfine matrices.[9] It appears that spectra of $\mathbf{3a}^-$ in CH_2Cl_2/THF or $CH_2Cl_2/C_2H_4Cl_2$ and $\mathbf{3b}^-$ in THF have Gaussian components (Figure 1d), whereas the components for

(3) Mao, F.; Philbin, C. E.; Weakley, T. J. R.; Tyler, D. R. *Organometallics* **1990**, *9*, 1510.
(4) (a) Fenske, D.; Becher, H. J. *Chem. Ber.* **1974**, *107*, 117. (b) Fenske, D. *Chem. Ber.* **1979**, *112*, 363.
(5) Kuchen, W.; Buchwald, H. *Chem. Ber.* **1959**, *92*, 227.
(6) Yang, K.; Bott, S. G.; Richmond, M. G. *Organometallics* **1994**, *13*, 3788.
(7) Yang, K.; Bott, S. G.; Richmond, M. G. *Organometallics* **1994**, *13*, 3767.
(8) (a) Mayr, A.; McDermott, G. A.; Dorries, A. M. *Organometallics* **1986**, *4*, 808. (b) McDermott, G. L.; Dorries, A. M.; Mayr, A. *Organometallics* **1987**, *6*, 925.
(9) Atherton, N. M. *Electron Spin Resonance*; Ellis Horwood: Chichester, 1973; pp 44-45.

Table 1. EPR Parameters for Metal Complexes

	solvent	g^b	$\lvert a^P\rvert/G^b$ $d\lvert a^P\rvert/dT^c$	$\lvert a^{Co}\rvert/G^d$ $d\lvert a^{Co}\rvert/dT^c$	w_0/G^e dw_0/dT^c	$w_{\pm1}/G^e$ $dw_{\pm1}/dT^c$
1[f]	THF	2.0042	11.047 ± 0.005 −4.3 ± 0.1	1.299 ± 0.001 1.57 ± 0.01[g]		
2[f]	THF	2.0038	9.69 ± 0.01 −2.7 ± 0.2	≤0.26		
3a$^-$	DCE/DCM	2.0036	7.939 ± 0.004 −2.0 ± 0.1	0.031 ± 0.001 0.01 ± 0.01	0.58 ± 0.08 −0.6 ± 1.4	0.47 ± 0.06 −1.5 ± 1.1
3a$^-$	DCM/THF	2.0034	8.00 ± 0.01 −2.2 ± 0.2	0.030 ± 0.001 0.02 ± 0.01	0.34 ± 0.07 −4 ± 1	0.26 ± 0.06 −5 ± 1
3a$^-$	THF	2.0036	8.066 ± 0.004 −2.7 ± 0.1	0.057 ± 0.002 −0.21 ± 0.05	0.33 ± 0.02[i] −1.2 ± 0.3	0.30 ± 0.01[i] −1.2 ± 0.3
3b$^-$	THF	2.0039	8.20 ± 0.02 −3.6 ± 0.3	0.09 ± 0.01 −0.8 ± 0.2	0.7 ± 0.1 0 ± 1	0.7 ± 0.1 2 ± 2
4$^-$	DCM/THF	2.0035	9.24 ± 0.02 −3.6 ± 0.3	0.141 ± 0.005[j] −0.02 ± 0.08	0.23 ± 0.04[i] −1.8 ± 0.6	0.25 ± 0.05[i] −1.2 ± 0.9
5$^-$	DCE/DCM	2.0044	8.644 ± 0.006 −3.8 ± 0.2		0.39 ± 0.03 −1.4 ± 0.8	0.39 ± 0.03 −1.2 ± 0.8

[a] Coupling to two equivalent ^{31}P nuclei at 300 K. [b] Uncertainty, ±0.0002. [c] In units of mG K^{-1}. [d] Coupling to one ^{59}Co nucleus at 300 K (unless otherwise noted). [e] Peak-to-peak derivative width of components of $m = 0$ or ±1 lines; Gaussian lines unless otherwise noted. [f] From ref 1. [g] +(0.014 ± 0.001 mG K^{-2}) (T − 300). [h] +(0.032 ± 0.004 mG K^{-2}) (T − 300). [i] Lorentzian line shapes. [j] Two ^{59}Co nuclei.

3a$^-$ in THF and **4**$^-$ in CH_2Cl_2/THF are more nearly Lorentzian (Figure 1e). Most spectra contain small satellite lines (see below) which may confuse the distinction between Gaussian and Lorentzian component shapes (note that the **3b**$^-$ line shown in Figure 1a,d shows such satellites). Furthermore, there is a strong cross-correlation in the least-squares fits between the unresolved ^{59}Co coupling and the component line widths. However, in almost all cases, the fitting routine converged to give similar results at all temperatures for spectra of **3a**$^-$, **3b**$^-$, and **4**$^-$ in a given solvent.

All spectra showed a relatively large dependence of the ^{31}P coupling on temperature, −2 to −4 mG K^{-1}. The ^{59}Co coupling also increases with decreasing temperature for **3b**$^-$ and **3a**$^-$ in THF but is essentially temperature-independent for **3a**$^-$ in $CH_2Cl_2/C_2H_4Cl_2$ or CH_2Cl_2/THF and **4**$^-$. The fitted component widths show more scatter, but in general, the fitted widths for **3a**$^-$ and **3b**$^-$ are significantly greater than for **4**$^-$; the widths for **3a**$^-$ and **4**$^-$ increase with decreasing temperature, whereas those of **3b**$^-$ are nearly temperature-independent. Furthermore, the widths for **4**$^-$ are nearly the same for $m = 0$ and ±1 whereas the width of the $m = 0$ line for **3a**$^-$ and **3b**$^-$ is greater than that of the ±1 lines. Although line widths were not accurately measured for **1** and **2**, in general they increased with decreasing temperature. We will discuss these line width effects below.

Most of the spectra of **3**$^-$ and **4**$^-$ showed small satellite lines, usually symmetrically arranged. Most of these are reproducible and are probably ^{13}C satellites, but in a few cases they appear to be due to other BMA complexes, either present in the original sample or resulting from radical decomposition. In a single series of spectra of **3b**$^-$, a doublet of doublets was observed, comparable in intensity with the expected spectrum, with a_1 = 12.94 ± 0.01 G, a_2 = 13.91 ± 0.01 G (at 300 K), and somewhat different temperature coefficients, −6.2 ± 0.3 and −2.2 ± 0.2 mG K^{-1}, respectively. The lines were relatively sharp with no evidence of unresolved ^{59}Co coupling. The identity of the species remains a mystery.

In almost all cases, on continued electrolysis and/or on standing of electrolyzed solutions of **3**$^-$ and **4**$^-$, the characteristic triplet-of-octets spectrum of **1** was observed. The measured coupling constants correspond within experimental error to those reported[1] for **1** in the same solvent and at the same temperature. The spectrum of **1** could be made much more prominent by reversing the electrolysis leads briefly, suggesting that **1** results from decomposition of an oxidation product. Since the anode and cathode of the in situ electrolysis cell are relatively close together, diffusion of **1** (or **1**$^+$) from the anode into the cavity is expected with time. Cyclic voltammograms of **3** and **4** show a small reduction peak on the cathodic scan after traversing the partially reversible oxidation.[6] This peak increases with decreasing scan rate, and, when the scan is reversed at −0.3 V, the corresponding oxidation peak is observed, $E_{1/2}$ = −0.04 V vs Ag wire. The present EPR evidence strongly suggests that this secondary oxidation product is **1**$^+$, consistent with the observed reversible oxidation of **1** at 0.07 V vs SCE.[10] Apparently **3**$^+$ or **4**$^+$ undergoes rapid Co−Co bond cleavage to form an unknown mononuclear species **X** and **1**$^+$:

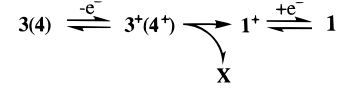

Co−Co bond cleavage is consistent with the expectation that the LUMO in **3** or **4** is the major Co−Co bonding orbital.[11,12] The process is thus reminiscent of the fragmentation of [μ-(PhCCPh)$Co_2(CO)_6$]$^-$ to [(PhCCPh)$Co(CO)_3$] and [$Co(CO)_4$]$^-$.[13]

EPR spectra of **5**$^-$, obtained by electrochemical reduction of **5** in 1:1 $CH_2Cl_2/C_2H_4Cl_2$, are triplets with relatively narrow Gaussian lines and a temperature-dependent ^{31}P coupling. The spectra were subjected to least-squares fitting as above; parameters are given in Table 1. Three pairs of satellites surround each major line. Although they may be ^{13}C satellites, they are much too weak to result from ^{183}W coupling ($I = {}^1/_2$, 14.3% abundant). Since the satellite widths increase with decreasing temperature more rapidly than do the major lines, it is likely that they result from other BMA complexes present as impurities in the original sample or resulting from decomposition of **5**$^-$.

The BMA Radical Anion. The room-temperature EPR spectrum of [BMA]$^-$ (**6**$^-$), prepared by [$CoCp_2$] reduction in THF, consists of the expected 1:2:1 triplet, corresponding to

(10) Mao, F.; Tyler, D. R.; Keszler, D. *J. Am. Chem. Soc.* **1989**, *111*, 130.
(11) Peake, B. M.; Rieger, P. H.; Robinson, B. H.; Simpson, J. *J. Am. Chem. Soc.* **1980**, *102*, 156.
(12) Thorn, D. L.; Hoffmann, R. *Inorg. Chem.* **1978**, *17*, 126.
(13) Arewgoda, M.; Rieger, P. H.; Robinson, J.; Visco, S. J. *J. Am. Chem. Soc.* **1982**, *104*, 5633.

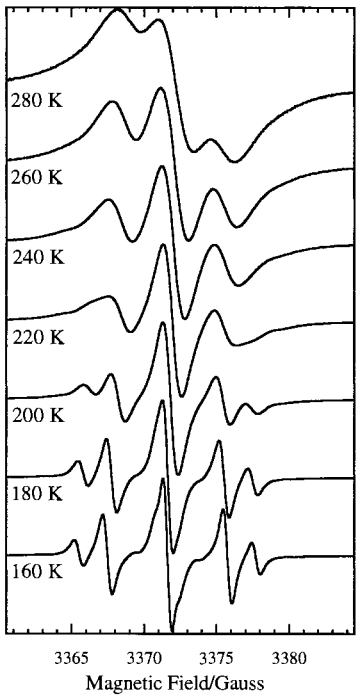

Figure 2. Experimental X-band EPR spectra of [BMA]$^-$ (**6**$^-$), 1 mM in THF, at 280−160 K.

hyperfine coupling of two equivalent ^{31}P nuclei. As the temperature is decreased, the spectrum changes, as shown in Figure 2. At first, the triplet resolution improves and the coupling constant increases in magnitude ($d|a|/dT = -10.8 \pm 0.3$ mG K^{-1}). However, at about 220 K, the outer lines of the triplet develop pronounced shoulders which resolve below 210 K, where the spectrum appears to be a superposition of two 1:2:1 triplets, **6a**$^-$ and **6b**$^-$, with the intensity of the spectrum of **6a**$^-$ 2−3 times the intensity of the spectrum of **6b**$^-$. Between 180 and 260 K, another pair of lines is partially resolved, corresponding to another apparent triplet spectrum (**6c**$^-$) with an amplitude less than 10% of **6a**$^-$. These features are not detectable below 180 K and merge into the broad major features at higher temperatures. The coupling constants of the two major spectra continue to increase with decreasing temperature. The relative intensities of the two major spectra remain nearly constant between 210 and 160 K. All spectra correspond to the same *g* value, 2.0035, independent of temperature.

At 160 and 170 K, shoulders are visible on the central line. Subtraction of a simulated spectrum of the **6a**$^-$ triplet shows that the spectrum of **6b**$^-$ is a doublet of doublets. Accordingly, all spectra in the 160-190 K range were analyzed by a nonlinear least-squares procedure which fitted the digitized experimental spectra to a simulation optimized with respect to B_0 (the same for **6a**$^-$ and **6b**$^-$), a_a, a_{b1}, a_{b2}, $K_{ba} = [\mathbf{6a}^-]/[\mathbf{6b}^-]$, the line widths, and, for the spectra at 180 and 190 K, a_c and $K_c = [\mathbf{6c}^-]/([\mathbf{6a}^-] + [\mathbf{6b}^-])$. The same procedure was used to analyze the spectra in the 240-280 K range, but only the average triplet coupling was determined. In all cases, the fitting errors were consistent with the experimental signal-to-noise ratio; to the eye, simulated spectra are indistinguishable from experimental spectra.[14] The resulting parameters are given in Tables 2 and 3. The temperature dependence of a^P is significantly different for the two spectra: −13 mG K^{-1} for **6a**$^-$ and −6 and −21 mG K^{-1} for **6b**$^-$. Satellite lines assignable to ^{13}C coupling are observed in the spectra at 160 K, an outer set with $a_c = 4.6$ G assignable to **6b**$^-$ and an inner set, visible only after subtraction of the simulated spectra from the experimental spectra, with $a_c = 4.2$ G assignable to **6a**$^-$.

(14) The line shapes in spectra of **6**$^-$ are clearly Lorentzian.

Table 2. ^{31}P Coupling Constants and Line Widths for **6**$^-$

		width[a]			
T/K	*a*/G	$m = 0$	$m = \pm 1$	K_c[b]	$a_{c/G}$
280	3.076(3)	2.86	3.05		
270	3.210(2)	2.22	2.39		
260	3.318(2)	2.34	2.45	0.051(1)	6.5(2)
240	3.516(4)	1.87	2.08	0.040(2)	5.7(2)

T/K	$a_{a/G}$	$a_{b/G}$	av width[a]	K_c	$a_{c/G}$
230	3.117[c]	5.82, 4.80[c]	1.36	0.034(6)	7.0(3)
220	3.265[c]	5.95, 4.89[c]	1.32	0.030(6)	7.2(3)
210	3.413[c]	6.08, 4.98[c]	0.94	0.036(5)	7.2(3)
200	3.555(3)	6.21(1), 5.08(1)	0.88	0.018(4)	7.5(3)
190	3.751(1)	6.133(4), 5.252(4)	0.75	0.004(2)	7.7(2)
180	3.878(1)	6.352(4), 5.328(4)	0.70	0.008(2)	8.2(1)
170	4.007(1)	6.565(3), 5.366(3)	0.63		
	4.009(1)	6.582(4), 5.355(4)	0.61		
160	4.142(2)	6.75(1), 5.45(1)	0.62		

[a] Peak-to-peak derivative width in gauss. [b] $K_c = [\mathbf{6c}]/([\mathbf{6a}] + [\mathbf{6b}])$. [c] Coupling constants extrapolated from lower temperatures used in determination of K_{ba}, k_{ab}, and K_c.

Table 3. Equilibrium and Rate Constants for the **6a**$^-$/**6b**$^-$ Equilibrium

T/K	$(10^{-6})k_{ab}$/s^{-1}	K_{ba}
230	9.4(2)	2.55(2)
220	5.6(1)	2.59(3)
210	3.51(5)	2.52(2)
200	1.94(3)	2.42(2)
190		2.68(2)
180		2.68(2)
170		2.85(2)
		2.92(2)
160		3.05(2)

Lines due to **6a**$^-$ and **6b**$^-$ coalesce in the temperature range 200-230 K. Detailed analysis of these spectra with the nonlinear least-squares procedure, modified to incorporate the modified Bloch equations,[15] yielded the equilibrium and rate constants for the **6a**$^-$/**6b**$^-$ equilibrium shown in Table 3. The coupling constants were fitted for the 200 K spectrum, but were held constant at values extrapolated from lower temperatures in fitting the 210, 220, and 230 K spectra. Again, the fitting errors were consistent with signal-to-noise ratios. From these four temperatures, we estimate the activation parameters $\Delta H_{ab}^{\ddagger} = 18.2 \pm 0.4$ kJ mol^{-1} and $\Delta S_{ab}^{\ddagger} = -30 \pm 2$ J mol^{-1} K^{-1}. Including the equilibrium constants at 160−190 K, we have $\Delta H_{ba}^{\circ} = -0.8 \pm 0.2$ kJ mol^{-1} and $\Delta S_{ba}^{\circ} = 4 \pm 1$ J mol^{-1} K^{-1}, i.e., **6a**$^-$ corresponds to slightly lower energy and higher entropy than **6b**$^-$.

Spectra of **6**$^-$ were recorded at 10° intervals, half going down in temperature, the other half coming back up. Since the collection of spectra form a smoothly varying set, the temperature effects are completely reversible, and there is no evidence of radical decomposition. This suggests that all three of the observed spectra correspond to conformations of the radical anion. The two major conformations, **6a**$^-$ and **6b**$^-$, correspond to very similar energies, but **6c**$^-$ apparently corresponds to a higher energy conformation since K_c increases with increasing temperature (a van't Hoff analysis is precluded by the low precision of the K_c values).

(15) The analysis included the spectrum of **6c**$^-$, assumed to be a triplet, but only for the purposes of overlap corrections; i.e., **6c**$^-$ was assumed to be only slowly exchanging with **6a**$^-$ and **6b**$^-$.

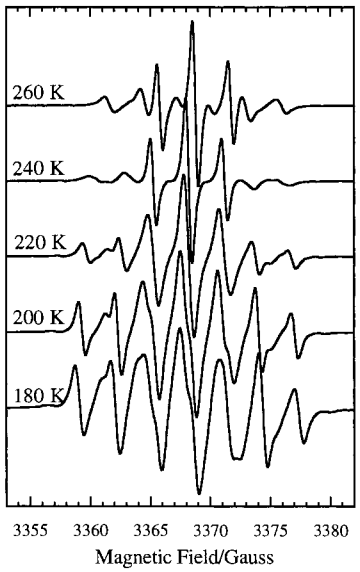

Figure 3. Experimental X-band EPR spectra of $[BPCD]^-$ ($\mathbf{7}^-$), 1 mM in THF, at 260−180 K.

The BPCD Radical Anion. The EPR spectrum of $\mathbf{7}^-$ at 260 K, prepared by electrochemical reduction in THF, consists of the expected triplet of triplets, corresponding to hyperfine coupling by two equivalent ^{31}P and two equivalent ^1H nuclei. As the temperature is decreased, the spectrum changes, as shown in Figure 3. This radical anion is considerably less stable than $\mathbf{6}^-$, and it was necessary to electrolyze continuously to obtain spectra with reasonable signal-to-noise ratios. Spectra of solutions reduced at or near room temperature showed features due to unidentified decomposition products. The methylene proton coupling of 2.97 ± 0.05 G showed little temperature dependence, but the ^{31}P coupling increases with decreasing temperature. Spectra in the 250−280 K range gave $|a^P|$ (300 K) = 3.66 ± 0.08 G with $d|a|/dT = -14 \pm 3$ mG K^{-1}. At lower temperatures, the spectrum changes more rapidly with the growth of small shoulders and the partial splitting of the central triplet lines, suggesting a minor conformer with a poorly characterized spectrum and a major conformer with nonequivalent ^{31}P nuclei. The lines are generally broader at low temperatures than those of the $\mathbf{6}^-$ spectra, and this, together with the complication of the additional ^1H coupling, precludes a detailed analysis. Nonetheless, the qualitative behavior of $\mathbf{7}^-$ and $\mathbf{6}^-$ is similar, with evidence for two or more conformers at low temperature which rapidly interconvert as the temperature approaches 300 K.

Mechanics Calculations for BMA. In an attempt to understand the possible conformations available to BMA, we performed molecular mechanics calculations, using the CAChe Mechanics program,[16] starting with a somewhat idealized structure with C_{2v} symmetry based on the x-ray crystal structure of BMA.[17] In the calculations, the maleic anhydride and phosphorus atoms were locked in position, all C−P−C bond angles and the bond lengths and bond angles of the phenyl rings were locked, and the torsional rotations of the phenyl rings were optimized as a function of the C−P−C═C dihedral angles. The results of these calculations are shown in the potential energy

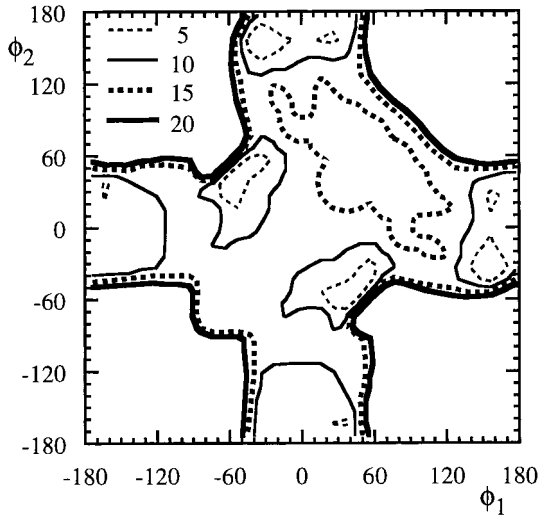

Figure 4. Potential energy contour map for BMA, determined by molecular mechanics calculations. The angles ϕ_1 and ϕ_2 represent the average C═C−P−C dihedral angles for Ph_2P_1 and Ph_2P_2, respectively. The energy of the most stable conformation ($\phi_1 = \pm 50°$, $\phi_2 = \mp 50°$) is set equal to 0. The corners of the map, bounded by the 20 kJ mol^{-1} contour line, correspond to much higher energies.

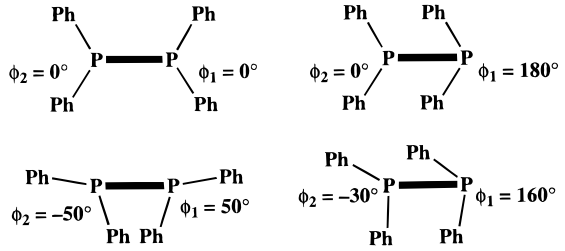

Figure 5. Schematic representations of the idealized "cis, cis" ($\phi_1 = \phi_2 = 0°$) and "cis, trans" (0°, 180°) conformations of BMA and the conformations found at the energy minima of Figure 4.

contour map of Figure 4. The angles ϕ_1 and ϕ_2 correspond to the average of the two C−P−C═C dihedral angles for P_1 and P_2, respectively, with $\phi_1 = 0°$ corresponding to the phenyl rings on P_1 oriented away from P_2 (phenyl rings cis to the nearest carbonyl group); similarly $\phi_2 = 0°$ corresponds to the phenyl rings on P_2 oriented away from P_1. To a first approximation, the two most stable conformations correspond to $\phi_1 = \phi_2 = 0°$ (the cis, cis conformation) and to $\phi_1 = 0$, $\phi_2 = 180°$ or $\phi_1 = 180$, $\phi_2 = 0°$ (the cis, trans conformation), Figure 5. The conformations near $\phi_1 = \phi_2 = 180°$ (trans, trans) have very much higher energies. Relatively small distortions from these idealized minima optimize the van der Waals interactions between phenyl rings; thus Mechanics finds minima at $\phi_1 \approx \pm 50$, $\phi_2 \approx \mp 50°$ and at $\phi_1 \approx 160$, $\phi_2 \approx -30°$ or vice versa. These minima differ by less than 1 kJ mol^{-1} and are separated by a barrier on the order of 12−15 kJ mol^{-1}, in surprisingly good agreement with the analysis of the experimental spectra described above. Two other minima at only slightly higher energies are found near the cis, trans idealized conformation.

Recognizing that the mechanics calculations correspond to the gas phase neutral molecule and that solvent interactions are doubtless important in stabilizing conformations of the radical anion and contributing to the activation barrier for interconversion of conformations, the results are nonetheless consistent with the EPR results, at least for the two major conformations. The cis, cis conformation has equivalent P atoms, and the energy minimum is broad. The cis, trans conformation has nonequiva-

(16) CAChe Scientific, Inc., Beaverton, OR; the computations described here utilized MM2 parameters and the block-diagonal Newton Raphson method to optimize structures, iterating until the energy change was less than 0.01 kJ mol^{-1}.

(17) Avey, A.; Schut, D. M.; Weakley, T. J. R.; Tyler, D. R. *Inorg. Chem.* **1993**, *32*, 233.

lent P atoms, and the energy minimum is somewhat sharper, corresponding to slightly lower entropy. Thus it seems reasonable to assign **6a**$^-$ to the *cis, cis* conformation and **6b**$^-$ to the cis, trans conformation. The third minor conformation remains unassigned.

Origins of the Phosphorus Hyperfine Coupling. Since the unpaired electron resides primarily in a O═C−C═C−C═O π* orbital, the ^{31}P coupling most likely arises from (i) polarization of P s orbitals by pπ spin density on the adjacent C atom and (ii) the direct contribution of P 3s character in the singly occupied MO, as shown by eq 1. The polarization parameter $Q_C{}^P$ is probably negative, but it has not been estimated either

$$a^P = Q_C{}^P \rho_C{}^\pi + Q_P{}^P \rho_P{}^{3s} \quad (1)$$

theoretically or experimentally. The corresponding parameter describing polarization of *P n*s orbitals by dπ spin density on Cr has been estimated at −40 G;[18] the shorter C−P bond suggests a significantly larger value for $Q_C{}^P$, say −60 G. Extended Hückel MO calculations on BMA suggest a π spin density on the order of 0.2 on the C atoms to which the P atoms are bonded, and thus a predicted coupling on the order of −12 G, comparable to the low-temperature couplings for BMA metal complexes. Since the singly occupied MO is essentially the same in [BMA]$^-$ and in its metal complexes, the polarization contribution to the coupling should remain nearly constant.

The contribution of P 3s spin density is positive and potentially large, $Q_P{}^P = 4750$ G.[19] In the idealized cis, cis or cis, trans conformations with C_s symmetry, P 3s character is symmetry forbidden but becomes allowed as the symmetry is reduced. Using the minimum-energy conformations found from the mechanics calculations, EHMO calculations predict P 3s spin densities of 0.0035, 0.0035 for the +50°/−50° conformation (approximately cis, cis) and 0.0003, 0.0017 for the +160°/−30° conformation (approximately cis, trans), corresponding to predicted P 3s contributions of 17, 17 G and 1, 8 G, respectively. Extended Hückel calculations suggest that the P 3s character is even greater for many thermally accessible conformations of **3**$^-$. Although these predictions are extremely approximate, they are qualitatively consistent with the small, equivalent ^{31}P couplings for conformation **3a**$^-$ and the larger, nonequivalent couplings for conformation **3b**$^-$, and thus they support the assignments based on the Mechanics calculations.

Temperature Dependence of the Phosphorus Hyperfine Coupling. From the above discussion, it is clear that the temperature dependence of a^P for **6**$^-$ and **7**$^-$ arises from excursions into conformations far from C_s symmetry and the consequent increasing contribution of P 3s character with increasing temperature, i.e., the average observed coupling becomes less negative. The phenomenon is thus analogous to the temperature dependence of the H coupling in aromatic hydrocarbon radicals,[20] which arises through the C−H out-of-plane bending mode, wherein the proton experiences a time-averaged positive contact interaction with π spin density which partially cancels the negative spin polarization contribution; $[C_6H_6]^-$, for example, has $d|a^H|/dT = -0.36$ mG K^{-1}.

Many of the asymmetric conformations accessible for **6**$^-$ are excluded for metal complexes which must stay close to the cis, cis idealized conformation. Indeed, the temperature dependence of the **6**$^-$ and **7**$^-$ couplings, ca. −13 mG K^{-1}, is considerably greater than for the metal complexes, ca. −3 mG K^{-1}. Although reduced in range, many lower symmetry conformations for which P 3s character is allowed are nonetheless accessible for the metal complexes. For example, EHMO calculations predict a P 3s contribution of 2.4 G for the +10°/−10° conformation. We should also note that all EHMO calculations (as well as the mechanics calculations) constrained the P atoms to the plane of the O═C−C═C−C═O system; in the X-ray structure of **2**,[10] the BMA P atoms are displaced ca. 0.4 Å above and below the mean plane of the O═C−C═C−C═O system. In any case, thermal excursions from the minimum-energy conformation are expected to broaden the distribution of a^P and make the average less negative.

Line Width and Line Shape Effects. As the range of low-symmetry conformations increases with increasing temperature, we expect a decrease in $|a^P|$ for **6**$^-$, **7**$^-$, and the metal complexes. In addition, the instantaneous distribution of a^P is expected to increase in width with increasing temperature and very likely becomes quite asymmetric. The various line width and line shape effects observed in the EPR spectra thus depend on the rate of averaging of this (probably skewed) distribution.

Examination of the line widths in spectra of **6**$^-$ as functions of temperature is revealing. In general, the widths increase with increasing temperature. At 160 K, the peak-to-peak line widths are about 0.6 G, nearly independent of m_I, suggesting negligible g and hyperfine anisotropy. As the temperature increases, however, the widths of the outer lines of the triplet and, to a lesser extent, the width of the central line increase significantly until, at 280 K, the triplet spectrum is only barely resolved. The spin-rotational interaction, the most common line width contribution which increases with increasing temperature, may be ruled out in this case since this effect is proportional to the g-matrix anisotropy[21] and in any case would not affect the hyperfine components unequally. At 280 K, line width contributions from the **6a**$^-$/**6b**$^-$ exchange process are negligible, but of course many other conformations are being explored at this temperature. The rate of exchange among these conformations must increase with increasing temperature, and indeed the lines remain Lorentzian, so that there is substantial motional narrowing. However, the width of the a^P distribution apparently increases faster than the rate of averaging.

The problem of motional averaging of a Gaussian distribution has been addressed by Freed.[22] He found that the absorption line shape can be expressed by an expansion in Lorentzian functions, as shown in eq 2, where Δ is the Gaussian width parameter, τ^{-1} is a measure of the rate of averaging, and ω_0 is the center frequency of the absorption line. In practice, eq 2

$$I(\omega) = \frac{e^{\Delta^2\tau^2}}{\pi} \sum_{n=0}^{\infty} \frac{(-1)^n}{n!} (\Delta\tau)^{2n} \frac{\frac{n}{\tau} + \Delta^2\tau}{\left(\frac{n}{\tau} + \Delta^2\tau\right)^2 + (\omega - \omega_0)^2} \quad (2)$$

converges for $\tau\Delta \leq 4$ with 70−80 terms in the sum. Line shapes, computed using eq 2, are shown in Figure 6 for $\tau\Delta =$ 0.25, 1, and 4. Also shown in Figure 6 are the correlation coefficients, r^2, for the fits of purely Gaussian or Lorentzian line shapes to the line shape computed from eq 2 as functions of $\tau\Delta$, with an approximate extrapolation for $\tau\Delta > 4$. Gaussian

(18) Cummings, D. A.; McMaster, J.; Rieger, A. L.; Rieger, P. H. *Organometallics* **1997**, *16*, 4362.
(19) Morton, J. R.; Preston, K. F. *J. Magn. Reson.* **1978**, *30*, 577.
(20) (a) Lawler, R. G.; Fraenkel, G. H. *J. Chem. Phys.* **1968**, *49*, 1126. (b) Reddoch, A. H.; Dodson, C. L.; Paskovich, D. H. *J. Chem. Phys.* **1970**, *52*, 2318.
(21) Atkins, P. W.; Kivelson, D. *J. Chem. Phys.* **1966**, *44*, 169.
(22) Freed, J. H. In *Electron Spin Relaxation in Liquids*; Muss, L. T., Atkins, P. W., Eds.; Plenum: New York, 1972; p 165.

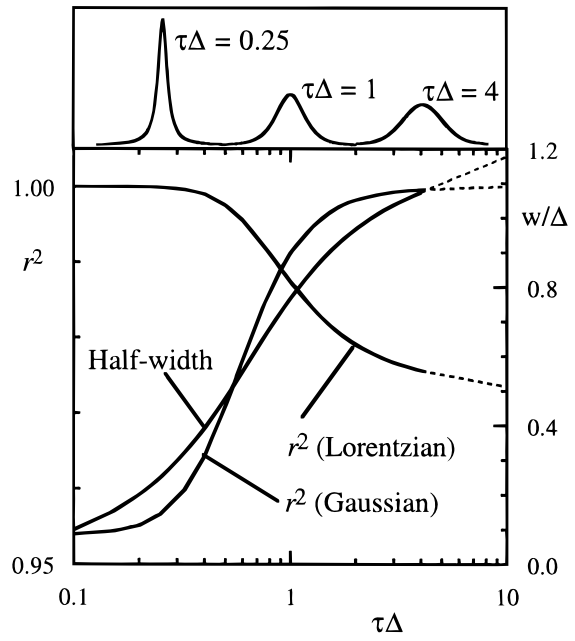

Figure 6. (top) Absorption line shapes, computed using eq 2, for $\tau\Delta = 0.25$, 1, and 4. (bottom) Plots of absorption line half widths at half height and correlation coefficients (r^2) for fits of purely Gaussian and purely Lorentzian line shapes to absorption lines computed using eq 2, all as functions of $\tau\Delta$.

line shapes are expected from eq 2 for $\tau\Delta > 2$ and Lorentzian line shapes for $\tau\Delta < 0.5$; for $\tau\Delta \approx 1$, the line shape is midway between Gaussian and Lorentzian. Thus the observation of Gaussian or Lorentzian line shapes in the experimental spectra is an indication of the rate of averaging relative to the width of the distribution. For relatively slow averaging, some motional narrowing is possible while retaining approximately Gaussian lines, while for relatively rapid averaging, Lorentzian lines may be observed but with rather large widths.

If the ^{31}P coupling were distributed in a Gaussian pattern, somewhat exchange narrowed to provide Lorentzian line shapes, and the two ^{31}P couplings were correlated in phase such that $a_1 - a_2 \approx 0$ at all times, the central line of the triplet would be sharp and the outer lines broadened; similarly an out-of-phase correlation with $a_1 + a_2 \approx$ constant would result in a broad central line and sharp outer lines.[23] If a_1 and a_2 are not correlated at all, the Gaussian distributions of $\pm(a_1 \pm a_2)/2$ would be identical with widths $1/2^{1/2}$ times than that of the a^P distribution, i.e., the widths of the inner and outer lines would be the same. On the other hand, our discussion above suggests that the distribution of a^P may well be skewed, with a broad tail into positive couplings as shown in Figure 7. In this case, the distribution of $\pm(a_1 - a_2)/2$ would be symmetric and somewhat narrower than the skewed distribution of $\pm(a_1 + a_2)/2$, as shown in the figure. Of course, these distributions are somewhat exchange-narrowed and the experimental spectra have Lorentzian shapes, but the difference in width will persist for moderate rates of averaging. The actual situation may well be a combination of a skewed distribution in a^P and partial in-phase correlation of a_1 and a_2.

(23) These effects are analogous to the "alternating line width effects" observed in EPR spectra of the dinitrodurene anion radical[24] and the durosemiquinone cation radical,[25] where steric effects lead to trapping of the unpaired electron on one nitro group or slow the rate of conformational averaging of the hydroxyl groups.
(24) Freed, J. H.; Fraenkel, G. K. *J. Chem. Phys.* **1963**, *39*, 326.
(25) Bolton, J. R.; Carrington, A. *Mol. Phys.* **1962**, *5*, 161.

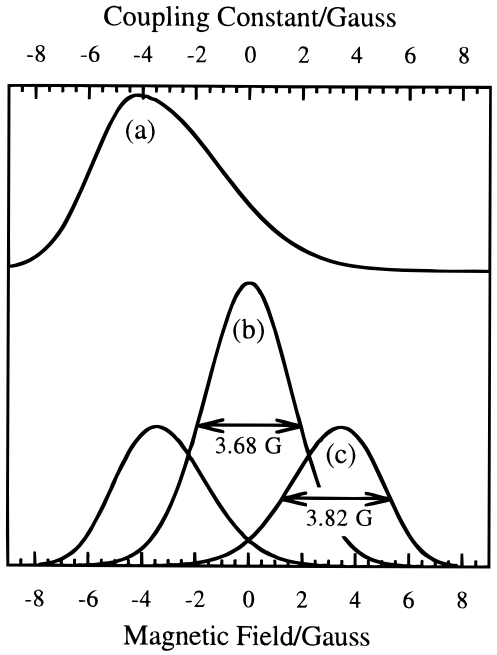

Figure 7. (a) Skewed distribution of a^P with $\bar{a} = -3$ G and the resulting distributions of (b) $\pm(a_1 - a_2)/2$ and (c) $\pm(a_1 + a_2)/2$.

In spectra of the metal complexes, line widths generally decrease with increasing temperature, but the line shapes are variable with Gaussian lines observed for **1**, **2**, **3a**$^-$ in CH_2Cl_2/$C_2H_4Cl_2$ or CH_2Cl_2/THF, **3b**$^-$, and **5**$^-$ and Lorentzian lines for **3a**$^-$ in THF and **4**$^-$. If the a^P distribution increases in width with increasing temperature, a decrease in line width suggests that the rate of averaging increases faster than the increase in the width of the distribution. This model is consistent when motional averaging is fast enough that the lines are Lorentzian, but as we have shown above, for somewhat slower motional averaging, the line width may decrease but the line remain essentially Gaussian in shape.

In the case of the metal complexes, *g*-matrix anisotropy is expected to the extent that metal orbitals participate in the singly occupied MO. Indeed, frozen solution spectra of **1** show such anisotropy[1] and isotropic spectra at low temperatures have quite broad lines as this anisotropy is averaged slowly. Frozen solution spectra of **3**$^-$ and **4**$^-$ are broad triplets with no hint of *g* anisotropy; nonetheless, this contribution may have a small but significant effect on the temperature dependence of the line widths of isotropic spectra.

It is interesting to note the appearance of Lorentzian lines for **4**$^-$ in the same solvent where **3a**$^-$ gives Gaussian lines. Lorentzian line shapes, associated with faster motional averaging, may be due to the expected greater flexibility of the six-membered ring of the bridging complex **4**$^-$ compared with the five-membered ring of the chelate complex **3a**$^-$. We also note that, for the bridging complex **4**$^-$, the $m = 0$ and ±1 lines have the same width, whereas the ±1 lines are broader for the chelating complexes, **3**$^-$. The broader $m = 0$ lines for the chelate complexes suggest that the two ^{31}P nuclei may be slightly nonequivalent, even when averaged; this is expected for **3**$^-$ where one P atom is trans to Co and the other trans to one of the acetylene carbon atoms.

Summary

(1) Reduction of $[Co_2(PhCCR)(CO)_4(\eta\text{-BMA})]$, R = Ph (**3a**), H (**3b**), $[Co_2(PhCCPh)(CO)_4(\mu\text{-BMA})]$ (**4**), or $[PhCW(CO)_2(BMA)Cl]$ (**5**) gives stable radical anions, **3**$^-$, **4**$^-$, and **5**$^-$, which

exhibit EPR spectra with temperature-dependent hyperfine coupling to two equivalent ^{31}P nuclei and to one ($\mathbf{3}^-$) or two ($\mathbf{4}^-$) ^{59}Co nuclei. Oxidation of **3** or **4** leads to Co−Co bond cleavage with one of the products identified as $[Co(CO)_3(BMA)]^+$ ($\mathbf{1}^+$).

(2) Reduction of BMA (**6**) or BPCD (**7**) gives radical anions, $\mathbf{6}^-$ and $\mathbf{7}^-$, the EPR spectra of which exhibit complex temperature dependence. Detailed analysis of the $\mathbf{6}^-$ spectra, together with a mechanics calculation for **6**, leads to the identification of two conformational isomers corresponding to the symmetric and asymmetric arrangements of the PPh_2 groups. Line shape analysis results in thermodynamic and activation parameters for the interconversion of these rotational conformers.

(3) The ^{31}P couplings observed in EPR spectra of BMA metal complexes, as well as $\mathbf{6}^-$ and $\mathbf{7}^-$, results from a negative spin-polarization contribution, proportional to the π-spin density on the adjacent C atom, and a (potentially large) positive contribution from P 3s character in the singly occupied MO. The latter contribution is symmetry forbidden in idealized C_{2v} structures with the P atoms in the plane of the O═C−C═C−C═O group of BMA or BPCD, but becomes allowed at finite temperatures where the PPh_2 groups rotate or deviate from the plane of the π system. The a^P temperature dependences observed for BMA metal complexes, −2 to −4 mG K^{-1}, and for $\mathbf{6}^-$ and $\mathbf{7}^-$, −6 to −21 mG K^{-1}, thus result from the increase in P 3s character with increasing temperature as the PPh_2 groups explore conformations increasingly removed from ideality.

(4) With increasing temperature, the width of the distribution of instantaneous ^{31}P couplings increases more rapidly than the rate of averaging, leading to an increase in line widths in spectra of $\mathbf{6}^-$. Temperature effects on line widths and component shapes in spectra of the BMA metal complexes arise from similar, but relatively smaller, changes with temperature in the distribution of a^P and the rate of averaging.

Acknowledgment. We thank R. G. Lawler for helpful discussions and J. H. Freed for guiding us to his work on exchange-narrowing of Gaussian lines. We thank the Robert A. Welch Foundation (Grant No. B-1039) for grant support to M.G.R., the National Science Foundation for grant support to D.R.T., and the NSF/New Zealand Exchange Program for supporting six weeks' work by N.W.D. at Brown University.

IC980581H